The bridge between first-principles calculations and grand canonical Monte Carlo simulations: Morse and Lennard-Jones force fields

Kunjie Li[a]; Dapeng Cao[a]

[a] Division of Molecular and Materials Simulation, Key Laboratory of Nanomaterials, Ministry of Education, Beijing University of Chemical Technology, Beijing, P.R. China

PLEASE SCROLL DOWN FOR ARTICLE

Taylor & Francis
Taylor & Francis Group

The bridge between first-principles calculations and grand canonical Monte Carlo simulations: Morse and Lennard-Jones force fields

Kunjie Li and Dapeng Cao*

Division of Molecular and Materials Simulation, Key Laboratory of Nanomaterials, Ministry of Education, Beijing University of Chemical Technology, Beijing 100029, P.R. China

We use the modelled adsorbate (methane) and adsorbent (carbon nanotube) to explore the choice of site-to-site force fields in order to bridge the gap between first-principles calculation and grand canonical Monte Carlo. By using the mature classical Lennard-Jones potential-based results as benchmark, it is found if the first-principles calculation is performed at the higher MP2/6-311G∗∗ level, Morse potential model should be adopted to achieve the force field parameters. It is expected that this work provides useful information for the building of the multiscale simulation method and the selection of accurate force field models.

Keywords: first-principles calculations; grand canonical Monte Carlo simulation; Morse function; multiscale simulation approach; carbon nanotubes

1. Introduction

Due to the fast development of nanostructure materials, the properties of these materials need better understanding in a wide range of length and timescales [1]. Thus, a systematic approach is required to develop new materials [2]. Recently, the multiscale theoretical approach, which combines the first-principles calculations and the grand canonical Monte Carlo (GCMC) simulations, has been widely used to investigate gas adsorption (such as H_2, CH_4) in different porous materials, including silicon nanotube [3,4], $Li_{12}Si_{60}H_{60}$ fullerene composite [5], silicon carbide nanotube [6], boron nitride nanotube [7], carbon nanoscroll [8], covalent organic frameworks (COFs) [9–11], metal-organic frameworks (MOFs) [12–15] and pillared graphene [16]. In this multiscale theoretical method, the first-principles calculations were performed not only to obtain the binding energy between gas and the materials, but also to explore gas adsorption sites. By inputting the first-principles calculations into GCMC simulations, we can obtain the gas uptakes of these materials of interest under different thermodynamic conditions. In previous publications, although all investigators used the first-principles calculation to obtain the binding energy, the choice of different methods and basis sets would lead to the diversity of the calculated results.

In general, the second-order Møller–Plesset (MP2) perturbation theory, a kind of wave function-based method, is usually deemed to be the high-level approach, and could yield the more reliable results for the weak interactions. The good agreement of experiment and simulation indicated that the MP2 method with the cc-PVTZ basis set used by Xiang et al. [15] does yield the reliable binding interaction between H_2 and the MOF. However, the MP2 method needs much more computational consumption and cannot be applied for the large systems. As a result, an alternative less computational cost method, i.e. density functional theory (DFT) method, which does not consider the dispersion forces, was also used extensively. Among these DFT methodologies (including PW91, B3LYP and PBE) used in previous work, the PBE functional with the TVZPP basis set could give a similar result with the MP2 method [9,12–14]. The basis set superposition error (BSSE) is critically important to describe the non-bonding interactions [12] in the MP2 method, but is an unnecessary setting in the methods of PW91 and B3LYP [3,6,7]. Besides the methods of the first-principles calculations, the fitting of force field is also very important for the investigation of gas storage by the GCMC simulations.

In some cases, it is difficult to exactly reproduce the experimental results by computer simulations, due to the difference of the experimental sample and simulation assumption. Therefore, there are uninterrupted dissensions for the first-principles calculations and the force field fitting method, because the different basis sets and force field models will yield obviously different results. Accordingly, how to choose the basis sets and force field models is the key to efficiently apply the multiscale simulation method to the investigations of gas adsorption. The choice of the basis sets determines the accuracy of the binding energy between gas and host materials, while the

*Corresponding author. Email: cao_dp@hotmail.com

force field model is the bridge between the first-principles calculation and GCMC simulation.

In this work, we intend to explore the two issues of how to select the basis sets and force field model. Since methane is a non-polar molecule and it can be represented by classical potential efficiently, which can act as the benchmark to calibrate the results of the multiscale simulations, we selected methane as a model adsorbate. In addition, due to the simplicity and wide application of carbon nanotube (CNT), we choose the single-walled carbon nanotube (SWNT) as a model adsorbent. We obtain the potential energy surface of CH_4 on the SWNTs using the first-principles calculations. Then, the results are used to fit the Morse potential and Lennard-Jones (LJ) potential in order to describe the site-to-site interaction between methane and SWNTs. Furthermore, the results of classical LJ (CLJ) potential with the parameter from united atoms are regarded as the benchmark to evaluate the selections of the first-principles calculations methods and the force field models.

2. Computational method

In this work, we considered the CH_4 and (14,14) CNT system, where the diameter of the (14,14) CNT is 1.9 nm. For reducing computational consumption, the cluster model method, i.e. a curved graphite sheet taken from the (14,14) SWNT, was used in the first-principles calculation. The first-principles calculations, containing PW91 exchange-correlation functionals based on the generalised gradient approximation and MP2 methods, were performed by the Gaussian 03 program package [17]. Figure 1 shows a schematic diagram of the cluster model used in the first-principles calculation for the (14,14) SWNT. This model contains 24 framework carbon atoms, and all the terminals are saturated with H atoms. There are three typical adsorption sites on nanotube surfaces: on-top, bridge and hollow. Our configuration optimisation results showed that, among different adsorption orientations, methane adsorbed on the hollow sites with a C—H bond

vertical to the tube surface and other C—H bonds placed geometrical symmetry, is the most favourable adsorption mode for both inside and outside the SWNT. The optimised structures are also presented in Figure 1.

Figure 2 shows the potential energy curves of CH_4 interaction with the (14,14) CNT at three different adsorption sites with the basis sets MP2/6-311G** considering the BSSE. The interactions in hollow sites are stronger than top sites and bridge sites, which also prove that the hollow sites are the favourable adsorption sites. The binding energy is 1.937 kcal/mol outside the tube and 2.685 kcal/mol within the tube for the hollow site. With the potential energy curves, we could gain the exact adsorption position and binding energy.

In the first-principles calculation, different methods can yield different binding energies [18–20] for the methane adsorption on the CNTs. Moreover, by the same method, the different basis sets also produce the different results [20]. For appropriately selecting the basis set, we calculated the binding energy by the CLJ potential in the optimisation binding site, where the distance from the centre of hexahydric ring and the carbon atom of CH_4 is 3.6 Å. The CLJ potential parameters were $\varepsilon_{ff}/k_B = 148.1$ K (with k_B Boltzmann's constant) and $\sigma_{ff} = 0.381$ nm for methane interactions, and $\varepsilon_{ss}/k_B = 28.0$ K and $\sigma_{ss} = 0.34$ nm for carbon interactions [21], respectively. The parameters for the methane and carbon atom interactions, obtained from the Lorentz–Berthelot mixing rules, [22] are 62.2 K and 0.361 nm, respectively. Based on the CLJ potential, the calculated binding energy is 1.69 kcal/mol when methane is out of the (14,14) SWNT.

Table 1 shows the binding energies of CH_4 outside the (14,14) SWNT with PW91 and MP2 methods at the distance of 3.6 Å from the nanotube surface to the molecule. However, what we should mention is that the equilibrium distances are different at different quantum calculation levels, and also different with and without BSSE corrections. Here, we used different methods and
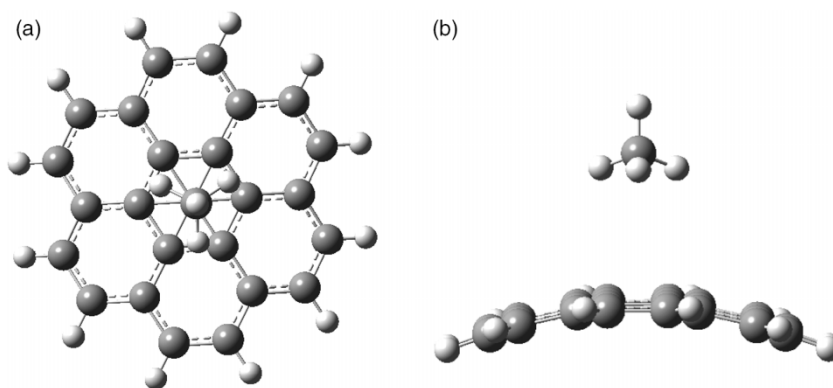

Figure 1.   Cluster model (hollow site) representing the (14, 14) CNT with the optimised structures: (a) top view and (b) side view.
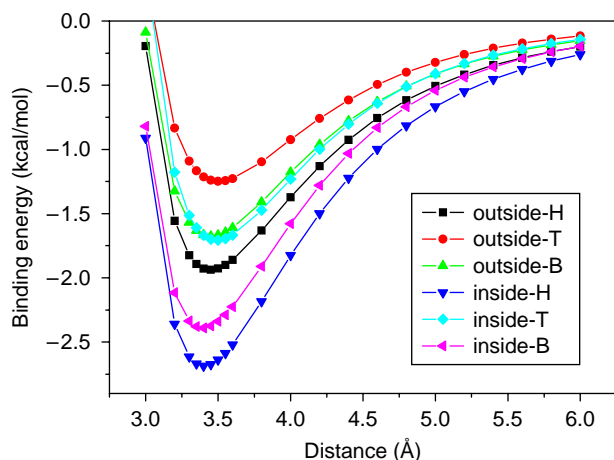
Figure 2. Potential energy curves of CH_4 adsorption in three sites of the tube wall of the (14,14) CNT: H, hollow; T, top and B, bridge.

basis sets at the optimisation-binding site to make a proper selection. For the PW91 exchange-correlation functional, the results are shown in Table 1(a) using a pair of basis sets. The CH_4 molecule and its nearest six carbon atoms are treated by different large basis sets (6-311G∗, 6-311G∗∗, 6-311 + G∗ and 6-311 + G∗∗), whereas the other atoms are treated by the commonly used small basis set 3-21G. It is found that the binding energy increases with the addition of the polarisation and diffusion functions in the basis sets. If one only adds the polarisation functions for atoms, the calculation-binding energies are almost the same, such as the 6-311G∗ (0.999 kcal/mol) and 6-311G∗∗ (1.027 kcal/mol) basis sets, as well as the 6-311 + G∗ (2.295 kcal/mol) and 6-311 + G∗∗ (2.299 kcal/mol) basis sets. Apparently, addition of the diffusion functions shows significant effect. Compared to 1.69 kcal/mol, the PW91 method with the four pairs of basis set could not give satisfactory results. If the BSSEs are considered, the binding energy exhibits an obvious decrease, about 20% of the no-BSSE results, which suggests that it is not necessary for the PW91 method to consider the BSSE. As the PW91 under-estimates the dispersion forces in molecules, the basis

sets plus the diffusion functions could be the compara-tively reasonable choice. For using only one basis set, shown in Table 1(b), the results from MP2 method are larger than the PW91 method based on the same basis set. By considering the BSSE, the MP2 method gives two acceptable results based on the 6-311G∗ (1.589 kcal/mol) and 6-311G∗∗ (1.859 kcal/mol) basis sets, compared to the CLJ result. So, it is relatively suitable to employ the PW91 method with the 6-311 + G∗∗ basis set and the MP2 method with the 6-311G∗ and 6-311G∗∗ basis sets in the first-principles calculations to describe our system.

In Figure 3, we present the comparison of potential energy curves of CH_4 adsorption in hollow sites for CLJ, PW91 methods without BSSE, and MP2 methods with BSSE. The results of the PW91 method show the same binding site as the CLJ out of the tube, where the distance from the centre of hexahydric ring and the carbon atom of CH_4 is 3.6 Å. However, the binding energy of the PW91 method (2.30 kcal/mol) is bigger than the CLJ (1.69 kcal/mol). Within the tube, the similar situation can be observed. The binding energy from the PW91 method is 3.22 kcal/mol, also bigger than the CLJ (2.09 kcal/mol). The binding sites in the MP2 methods exhibit a slight change nearer to the tube than the PW91 method. The binding energies based on 6-311G∗ and 6-311G∗∗ basis sets, are 1.61 kcal/mol (3.50 Å) and 1.94 kcal/mol (3.45 Å) out of the tube, respectively, while within the tube, they are 2.27 kcal/mol (3.45 Å) and 2.68 kcal/mol (3.40 Å). Apparently, the PW91 method is not good to describe the cases studied here. In fact, the long-range van der Waals (vdW) interactions between methane and CNTs play an important role in this work, while the DFT cannot describe the long-range electron correlations that are responsible for vdW dispersion forces. However, quantum chemistry techniques (MP2) can describe this long-range correlation effect. This may be the main reason for the difference using MP2 and PW91 methods. In addition, it is found from Figure 3 that the binding energies inside the tube are larger than the outside.

To feasibly bridge the gap between the first-principles calculation and the GCMC simulation, we used LJ and

Table 1. Binding energy (kcal/mol) of CH_4 outside the (14, 14) SWNT; results obtained from different basis sets: (a) the PW91 methods and (b) the PW91 and MP2 methods.

	PW91			PW91		MP2	
(a)	E	E-BSSE	(b)	E	E-BSSE	E	E-BSSE
–	–	–	6-31G∗	0.829	0.069	2.087	1.032
6-311G∗	0.999	0.276	6-311G∗	0.648	0.296	2.547	1.589
6-311G∗∗	1.027	0.283	6-311G∗∗	0.671	0.309	2.826	1.859
6-311 + G∗	2.295	0.456	6-311 + G∗	1.036	0.309	5.211	1.944
6-311 + G∗∗	2.299	0.470	6-311 + G∗∗	0.936	0.346	4.998	2.190

Note: E-BSSE means the binding energies are counterpoise corrected by BSSE. The values presented are in kcal/mol.
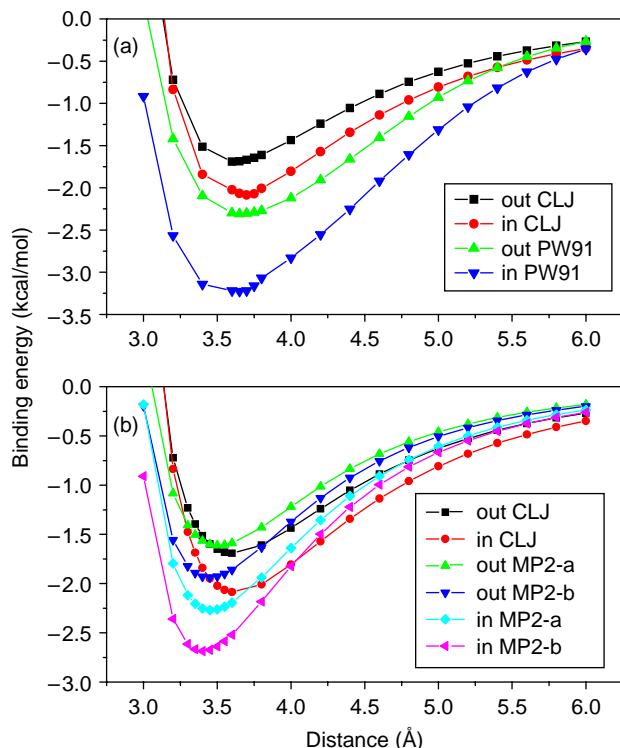
Figure 3. Comparisons of potential energy curves of CH_4 adsorption in hollow sites: (a) PW91 method and CLJ and (b) MP2 methods and CLJ. PW91 means a pair of basis sets: 3-21G and 6-311 + G**, MP2_a means the MP2/6-311G* basis set and MP2_b means the MP2/6-311G** basis set.

Morse potential functions to describe the interaction between the fluid molecule and the nanotube. The first-principles calculation results of CH_4 with SWNTs were, respectively, fitted to a LJ potential and a Morse potential by the site-to-site methods. In most research of newly emerging materials, like COFs and MOFs, the site-to-site method is necessary to represent the interactions between gas and different type atoms in the material. In our previous publications, [9–11], we investigated hydrogen storage in Li-doped COFs using multiscale approach, in which the first-principles calculation results have been successfully fitted into the Morse function via the site-to-site method, and then the input GCMC simulation for evaluating adsorption of hydrogen in Li-doped COFs. Therefore, here we mainly investigate which potential model is more reasonable in the site-to-site fitting method. In the LJ and Morse potential functions, methane molecule is treated as a pseudoatom with the centre of mass on the site of carbon atom, due to its non-polar spherical structure. For clear presentation, the Morse potential is given as follows:

$$U_i = 2D[x^2 - 2x], \quad x = \exp\left(-\frac{\gamma}{2}\left(\frac{r_i}{r_e}\right) - 1\right), \quad (1)$$

where r_i is the interaction distance in Å. D, γ and r_e denote the well depth, the stiffness (force constant) and the equilibrium bond distance, respectively.

To explore the effects of potential models (i.e. LJ and Morse potentials) on adsorption of gas, the simulations of methane adsorption in SWNT bundles at room temperature were performed using the GCMC method. In the GCMC simulation, the temperature, the chemical potential and the volume are specified. The LJ and Morse potentials were used in the GCMC simulations for comparison. SWNT bundles were arranged in a diamond array, with the 8 Å spacing between the tube walls of the neighbouring tubes [22]. The periodic boundary conditions were applied in the three dimensions. The cut-off radius was five times the collision diameter. An initial configuration was generated randomly before the GCMC simulation. For each state point, the GCMC simulation consisted of 1×10^7 steps to guarantee equilibration, and the following 1×10^7 steps were used to sample the adsorption amount.

3. Results and discussion

We used GCMC simulation to evaluate the adsorption of methane in the (14,14) CNT arrays at $T = 298$ K. By fitting the first-principles calculation results to potential models, the potential parameters obtained from site-to-site methods, were put into the GCMC simulation to represent the interaction between the methane and the carbon atoms or the tube surface. The excess gravimetric and volumetric adsorption capacities were calculated. All the adsorption data were compared with the results based on the CLJ potential, where the CLJ potential used in the GCMC simulation, is also the site-to-site method. The calculated maximal excess adsorption capacity is 168 g CH_4/kg C and 169 v/v at $P = 6$ MPa. Our calculation result is comparable to the one of 160 v/v at 3.5 MPa and 303 K reported by Kaneko and co-workers [23]. Considering the difference of the conditions and methods, it is believed that the CLJ-based GCMC data are reasonable, and could be used as the benchmark to calibrate our fitted force fields-based GCMC results.

In this section, we mainly compare the results from the CLJ and the ones fitted by the site-to-site method. Figure 4 shows the methane excess adsorption capacity at $T = 298$ K and $P = 1$–8 MPa, where the binding energy is taken from the first-principles calculations at the MP2/6-311G* level. The Morse-fitting and LJ-fitting indicate that the potential energy curves of the first-principles calculations were fitted into the Morse and LJ models, and the obtained parameters subsequently acted as input of the GCMC simulations. It can be found from Figure 4 that the methane uptakes obtained by LJ-fitting method are in excellent agreement with the CLJ results, while the uptakes obtained by Morse-fitting method are significantly smaller than the CLJ results. In particular, at $P = 6$ MPa, the excess gravimetric and volumetric uptakes from
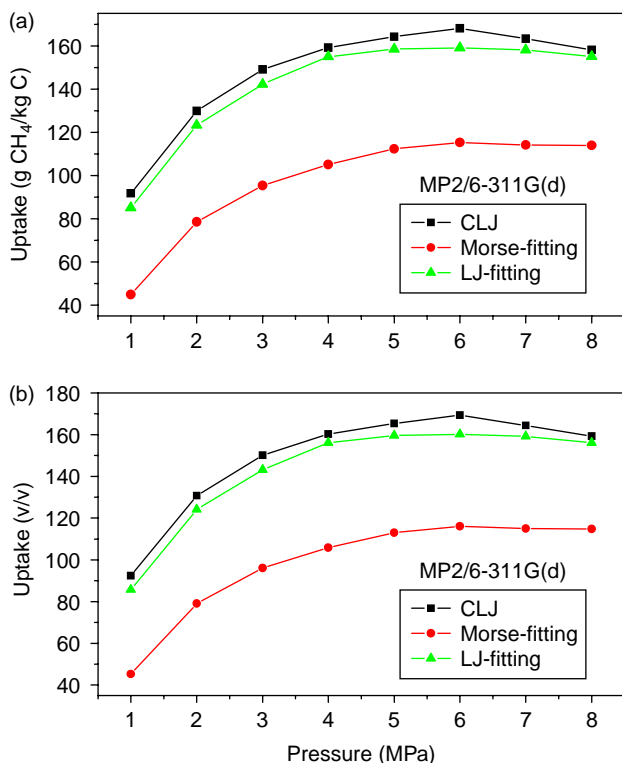
Figure 4. Methane excess adsorption capacity at $T = 298$ K, where force fields are from the MP2/6-311G∗ method.
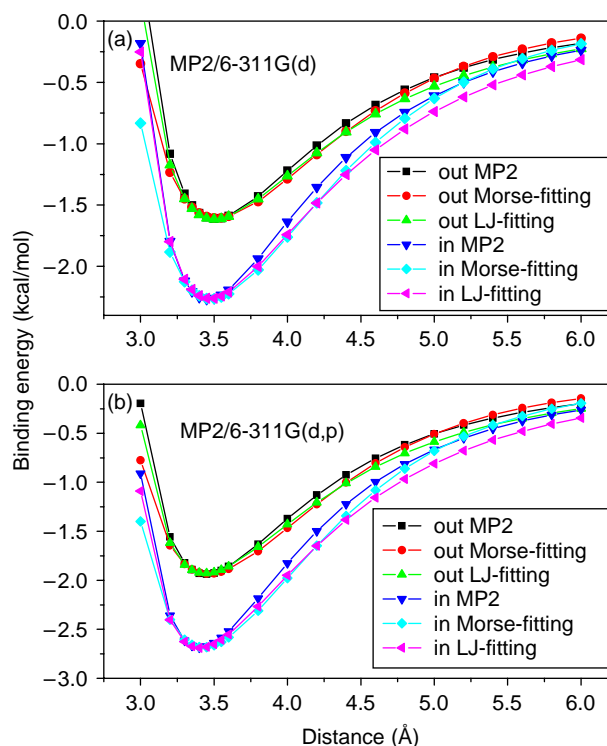

Figure 5. Force fields from the LJ-fitting and Morse-fitting by site-to-site method: (a) at the level of MP2/6-311G∗ and (b) at the level of MP2/6-311G∗∗: out (outside) and in (inside).

LJ-fitting method are 159 g CH_4/kg C and 160 v/v, which are close to 168 g CH_4/kg C and 169 v/v from the CLJ potential, while the ones from Morse-fitting method are 115 g CH_4/kg C and 116 v/v, respectively. Obviously, if the MP2/6-311G∗ method is used in the first-principles calculations, we should use the site-to-site LJ-fitting to obtain the force field parameters.

Figure 5(a) shows the force fields from the LJ-fitting and Morse-fitting by the site-to-site method and the first-principles calculation results at the level of MP2/6-311G∗. The equilibrium tube-molecule distance is 3.5 and 3.45 Å based on the MP2/6-311G∗ level, respectively, outside and inside of the (14,14) CNT. At this binding site, the force fields, both from LJ-fitting and Morse-fitting, are in excellent agreement with the first-principles calculation results. However, when CH_4 molecule departs from this equilibrium site, both of the force fields give a slight deviation from the first-principles calculation results. Apparently, it can be observed from Figure 5(a) that the width of the LJ potential is larger than the Morse potential, which may be the reason for the difference of the two force field-based GCMC results.

Figure 6 shows the methane excess adsorption capacity at $T = 298$ K, where binding energy is taken from the first-principles calculations at the MP2/6-311G∗∗ level. In this case, the adsorption isotherm of methane obtained by

Morse-fitting method is slightly smaller than the CLJ results, and in basic agreement with the CLJ one, while the isotherm obtained by LJ-fitting method is significantly larger than the CLJ result. In particular, at $P = 6$ MPa, the excess gravimetric and volumetric uptakes from Morse-fitting method are 159 g CH_4/kg C and 159 v/v, which are close to 168 g CH_4/kg C and 169 v/v from the CLJ potential, while the ones from LJ-fitting method are 197 g CH_4/kg C and 199 v/v, respectively. Compared to the MP2/6-311G∗ method, if the MP2/6-311G∗∗ method is used in the first-principles calculations, we should use the site-to-site Morse-fitting to obtain the force field parameters. Actually, it coincides with our previous results that the site-to-site Morse-fitting produces the accurate adsorption isotherms of hydrogen in Li-doped COFs [11]. If the site-to-site LJ-fitting method is used, the adsorption of gas would be overestimated significantly.

Figure 5(b) shows the force fields from the LJ-fitting and Morse-fitting by the site-to-site method and the first-principles calculation results at the level of MP2/6-311G∗∗. Compared to the MP2/6-311G∗ level, the equilibrium tube-molecule distance changes to 3.45 and 3.4 Å based on the MP2/6-311G∗∗ level, respectively, outside and inside of the (14,14) CNT. Basically, the LJ-fitting and Morse-fitting force fields are in good agreement with the first-principles calculation results. However,
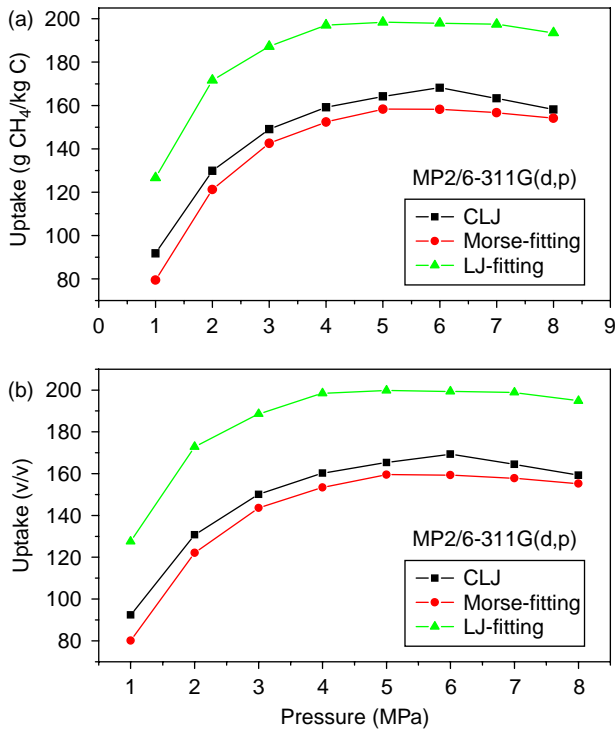
Figure 6. Methane excess adsorption capacity at $T = 298$ K, where force fields are from the MP2/6-311G** method.

apparently, Morse force field reflects the first-principles calculations more accurately, compared to the LJ-fitting force field.

Table 2 lists the parameters of the site-to-site LJ-fitting and Morse-fitting at MP2/6-311G* and MP2/6-311G** levels and the PW91 method. At the same MP2 level, the parameters ε and D have almost the same value in the LJ-fitting and Morse-fitting. The main difference is from the binding site, which is consistent with the observation from Figure 5. For the PW91 method, due to the bigger parameters, the binding energy is 2.30 kcal/mol outside the

Table 2. Parameters of the LJ potential and Morse potential fit by site-to-site from the results of MP2 and PW91 method.

	LJ		Morse		
	ε (kcal/mol)	σ (Å)	D (kcal/mol)	g	r_c (Å)
MP2/6-311G*					
Out	0.126	3.508	0.125	11.024	4.012
In	0.145	3.467	0.144	11.248	3.946
MP2/6-311G**					
Out	0.153	3.452	0.154	11.068	3.948
In	0.176	3.405	0.174	11.268	3.888
PW91					
Out	0.172	3.667	0.159	10.009	4.202
In	0.202	3.542	0.182	9.664	4.092
CLJ	0.128	3.605			

tube and 3.22 kcal/mol in the tube, which are 1.5 times larger than the CLJ results. Therefore, we believe that the PW91 method is not suitable for using in GCMC to investigate gas adsorption. Actually, if we adopt the PW91-based results to perform the site-to-site Morse-fitting and LJ-fitting to obtain the force field parameters, an absolutely overestimated uptake would be achieved, where the maximal excess gravimetric capacities reach 231.72 g CH_4/kg C for the Morse-fitting and 257.65 g CH_4/kg C for the LJ-fitting, which are unacceptable, because they are extremely larger than the CLJ result (168 g CH_4/kg C).

4. Conclusions

Owing to the diversity of atom types of novel materials, like COF and MOF, the site-to-site force field is commonly used to calculate the interaction between adsorbate and adsorbent. Here, by using methane and SWNT as adsorbate and adsorbent models, we investigate how to choose the force fields to bridge the gap between the first-principles calculations and the GCMC simulation. The PW91 and MP2 methods were applied to calculate the binding energy curves. By using the mature CLJ potential-based results as benchmark, it is found if the first-principles calculation is performed at the MP2/6-311G* level to obtain the binding energy, the LJ model should be adopted to get the force field parameters, while if the first-principles calculation is performed at the higher MP2/6-311G** level, Morse model should be adopted to achieve the force field parameters. It is expected that this work provides useful information for the building of the multiscale simulation method and the selection of accurate force field models.

References

[1] T.E. Karakasidis and C.A. Charitidis, *Multiscale modeling innanornaterials science*, Mater. Sci. Eng. C 27 (2007), pp. 1082–1089.
[2] T.S. Gates, G.M. Odegard, S.J.V. Frankland, and T.C. Clancy, *Computational materials: Mults-scale modeling and simulation of nanostructured materials*, Compos. Sci. Technol. 65 (2005), pp. 2416–2434.
[3] J. Lan, D. Cheng, D. Cao, and W. Wang, *Silicon nanotube as a promising candidate for hydrogen storage: From the first principle calculations to grand canonical Monte Carlo simulations*, J. Phys. Chem. C 112 (2008), pp. 5598–5564.
[4] G.P. Lithoxoos, J. Samios, and Y. Carissan, *Investigation of silicon model nanotubes as potential candidate nanomaterials for efficient hydrogen storage: A combined* Ab initio*/Grand canonical monte carlo simulation study*, J. Phys. Chem. C 112 (2008), pp. 16725–16728.

[5] J. Lan, D. Cao, and W. Wang, *Li12Si60H60 fullerene composite: A promising hydrogen storage medium*, ACS Nano 3 (2009), pp. 3294–3300.

[6] G. Mpourmpakis, G.E. Froudakis, G.P. Lithoxoos, and J. Samios, *Carbon nanoscrolls: A promising material for hydrogen storage*, Nano Lett. 6 (2006), pp. 1581–1583.

[7] G. Mpourmpakis and G.E. Froudakis, *Why boron nitride nanotubes are preferable to carbon nanotubes for hydrogen storage? An* ab initio *theoretical study*, Catal. Today 120 (2007), pp. 341–345.

[8] G. Mpourmpakis, E. Tylianakis, and G.E. Froudakis, Ab-initio *and monte-carlo investigation of hydrogen storage in carbon nanoscrolls*, Nano Lett. 7 (2007), pp. 1893–1897.

[9] J. Lan, D. Cao, W. Wang, T. Ben, and G. Zhu, *High-capacity hydrogen storage in porous aromatic frameworks with diamond-like structure*, J. Phys. Chem. Lett. 1 (2010), pp. 978–981.

[10] J. Lan, D. Cao, and W. Wang, *High uptakes of methane in Li-Doped 3D covalent organic frameworks*, Langmuir 26 (2010), pp. 220–226.

[11] D. Cao, J. Lan, W. Wang, and B. Smit, *Lithium-Doped 3D covalent organic frameworks: High-capacity hydrogen storage materials*, Angew. Chem. Int. Ed. 48 (2009), pp. 4730–4733.

[12] E. Klontzas, A. Mavrandonakis, G.E. Froudakis, Y. Carissan, and W. Klopper, *Molecular hydrogen interaction with IRMOF-1: A multiscale theoretical study*, J. Phys. Chem. C 111 (2007), pp. 13635–13640.

[13] S. Han, H. Furukawa, O.M. Yaghi, and W.A. Goddard III, *Covalent organic frameworks as exceptional hydrogen storage materials*, J. Am. Chem. Soc. 130 (2008), pp. 11580–11581.

[14] A. Mavrandonakis, E. Klontzas, E. Tylianakis, and G.E. Froudakis, *Enhancement of hydrogen adsorption in metal-organic frameworks by the incorporation of the sulfonate group: A multiscale computational study*, J. Am. Chem. Soc. 131 (2009), pp. 13410–13414.

[15] Z. Xiang, J. Lan, D. Cao, X. Shao, W. Wang, and D.P. Broom, *Hydrogen storage in mesoporous coordination frameworks: Experiment and molecular simulation,* J. Phys. Chem. C 113 (2009), pp. 15106–15109.

[16] G.K. Dimitrakakis, E. Tylianakis, and G.E. Froudakis, *Pillared graphene: A new 3-D network nanostructure for enhanced hydrogen storage,* Nano Lett. 8 (2008), pp. 3166–3170.

[17] M.J. Frisch, G.W. Trucks, H.B. Schlegel, G.E. Scuseria, M.A. Robb, J.R. Cheeseman, J.A.J. Montgomery, T. Vreven, K.N. Kudin, J.C. Burant, J.M. Millam, S.S. Iyengar, J. Tomasi, V. Barone, B. Mennucci, M. Cossi, G. Scalmani, N. Rega, G.A. Petersson, H. Nakatsuji, M. Hada, M. Ehara, K. Toyota, R. Fukuda, J. Hasegawa, M. Ishida, T. Nakajima, Y. Honda, O. Kitao, H. Nakai, M. Klene, X. Li, J.E. Knox, H.P. Hratchian, J.B. Cross, V. Bakken, C. Adamo, J. Jaramillo, R. Gomperts, R.E. Stratmann, O. Yazyev, A.J. Austin, R. Cammi, C. Pomelli, J.W. Ochterski, P.Y. Ayala, K. Morokuma, G.A. Voth, P. Salvador, J.J. Dannenberg, V.G. Zakrzewski, S. Dapprich, A.D. Daniels, M.C. Strain, O. Farkas, D.K. Malick, A.D. Rabuck, K. Raghavachari, J.B. Foresman, J.V. Ortiz, Q. Cui, A.G. Baboul, S. Clifford, J. Cioslowski, B.B. Stefanov, G. Liu, A. Liashenko, P. Piskorz, I. Komaromi, R.L. Martin, D.J. Fox, T. Keith, M.A. Al-Laham, C.Y. Peng, A. Nanayakkara, M. Challacombe, P.M.W. Gill, B. Johnson, W. Chen, M.W. Wong, C. Gonzalez, and J.A. Pople, *Gaussian 03*, Gaussian, Inc., Wallingford, CT, 2004.

[18] J. Zhao, A. Buldum, J. Han, and J.P. Lu, *Gas molecule adsorption in carbon nanotubes and nanotube bundles*, Nanotechnology 13 (2002), pp. 195–200.

[19] A. Ricca, and C.W. Bauschlicher, Jr, *The physisorption of CH4 on graphite and on a (9,0) carbon nanotube,* Chem. Phys. 324 (2006), pp. 455–458.

[20] P.A. Denis, *Methane adsorption inside and outside pristine and N-doped single wall carbon nanotubes,* Chem. Phys. 353 (2008), pp. 79–86.

[21] R.C. Reid, J.M. Prausnitz, and B.E. Poling, *The Properties of Gases and Liquids*, McGraw-Hill, New York, 1987.

[22] D. Cao, X. Zhang, J. Chen, W. Wang, and J. Yun, *Optimization of single-walled carbon nanotube arrays for methane storage at room temperature,* J. Phys. Chem. B 107 (2003), pp. 13286–13292.

[23] E. Bekyarova, K. Murata, M. Yudasaka, D. Kasuya, S. Iijima, H. Tanaka, H. Kahoh, and K. Kaneko, *Single-wall nanostructured carbon for methane storage*, J. Phys. Chem. B 107 (2003), pp. 4681–4684.